metals

MDPI

Article

Study on Mass Transfer of Phosphorus Based on New Hot-Metal Dephosphorization Kinetic Model

Guobin Sun [1,*] and Xiaodong Xiang [1,2]

[1] College of Resource and Environmental Engineering, Wuhan University of Science and Technology, Wuhan 430081, China; xiaodong1958@126.com
[2] State Environmental Protection Key Laboratory of Mineral Metallurgical Resources Utilization and Pollution Control, Wuhan 430081, China
* Correspondence: wustcree@163.com

Abstract: To investigate mass transfer of phosphorus in hot-metal dephosphorization process, it is necessary to reduce the deviation of traditional dephosphorization models in fitting accuracy. According to the change in hot-metal phosphorus content during dephosphorization, a new dephosphorization model was established by introducing the concept of "dynamic relative area". With the help of literature data and comparative analysis of the new and old models, the rationality of the new model was verified. On this basis, in order to reveal the effects of CaO and its derivatives on mass transfer of phosphorus, based on the dephosphorization effect of Fe_tO–CaO–SiO_2–$CaCl_2$ slags on high-phosphorus hot metal at 1673 K (1400 °C), the mass transfer process of phosphorus was investigated by calculating, analyzing, and discussing the overall mass transfer coefficients of phosphorus using CaO, $Ca(OH)_2$, and $CaCO_3$ with equal molar amount as fixatives (slag formers) in dephosphorizer respectively. The results show that the overall mass transfer coefficients of phosphorus under the action of $Ca(OH)_2$ and $CaCO_3$ are 0.0216 cm/s and 0.0363 cm/s, respectively, which are significantly lower than 0.0840 cm/s under the action of CaO.

Keywords: hot metal; dephosphorization; kinetic model; mass transfer coefficients; calcium oxide; calcium hydroxide; calcium carbonate

Citation: Sun, G.; Xiang, X. Study on Mass Transfer of Phosphorus Based on New Hot-Metal Dephosphorization Kinetic Model. *Metals* **2022**, *12*, 751. https://doi.org/10.3390/met12050751

Academic Editors: Norman Toro, Edelmira Gálvez and Ricardo Jeldres

Received: 23 March 2022
Accepted: 21 April 2022
Published: 27 April 2022

1. Introduction

In industrial production, CaO is often used as a fixative in slag. However, because it is often exposed to the air or drenched by rain during storage or transportation, some CaO will inevitably produce $Ca(OH)_2$ [1]. Meanwhile, CaO is mostly made by calcining $CaCO_3$. When $CaCO_3$ particles are too large to burn through, some of them also inevitably remain in the CaO. So far, although the physicochemical properties, decomposition thermodynamics, and kinetics of $Ca(OH)_2$ and $CaCO_3$ have been fully researched [2–5], their effects on hot-metal dephosphorization have not been investigated yet. Therefore, it is valuable to reveal the effects of $Ca(OH)_2$ and $CaCO_3$ on mass transfer of phosphorus.

At present, many achievements have been made in research on mass transfer of phosphorus in hot metal, slag, or both phases [6–11]. Although these achievements have played an important role in research on dephosphorization kinetics, they still have defects in practical application. Among them, the deviation between the model curve and experimental data is a prominent problem. Most models can only ensure that the fitting curve is consistent with a few experimental data.

It was unusual that when the product of the interface area (A) and the overall mass transfer coefficient (k_O) was taken as the mass transfer parameter ($A \cdot k_O$), it was found that $A \cdot k_O$ would gradually decrease as dephosphorization reaction proceeded. In the explanation of this phenomenon, Manning et al. [12] proved that emulsification can increase the slag-iron interface area (A) through the existence of metal droplets in the slag. However, because the number of droplets entering the slag was small and it was not clear whether

they could return to the hot metal, their effect on the mass transfer parameter remains to be determined. Meanwhile, Diao [13,14] and Ji [15] proposed that flux (fluxing agent) can increase $A \cdot k_O$ in the early stage of dephosphorization by improving the fluidity of the initial slag, but this does not explain the difference of $A \cdot k_O$ in the early and late stages. In addition, according to Wang et al. [16], the increase in P_2O_5 content and the decrease in Fe_tO content in slag can reduce k_O by increasing slag viscosity, but their effect at high temperatures is not significant, so it is difficult to cause a sharp decrease in $A \cdot k_O$. It is worth mentioning that although Gu et al. [17] believe that CO generated in hot metal is easy to increase A and k_O through the stirring of bubbles. However, the oxidation sequence of carbon and phosphorus in hot metal is different in different dephosphorization processes, so it is not discussed at present.

In conclusion, these researchers did not explain the reasons for the deviation in data fitting. Although some explanations for the decrease in mass transfer parameter are reasonable to a certain extent, they have not been confirmed by establishing models. In view of this situation, according to the change in phosphorus content in hot metal during dephosphorization, a concept of "dynamic relative area" is proposed to establish a new dephosphorization kinetic model. Then, with the help of literature data, the rationality of the new model will be verified from the fitting accuracy and the characteristics of the mass transfer parameter. Finally, combined with a brief analysis, the new model will be applied to research the mass transfer of phosphorus under the action of CaO and its derivatives.

2. Experimental

2.1. Materials

The pig iron powder (melting point < 1400 °C) used in the experiments was obtained by mixing pure iron, ferrosilicon, ferrophosphorus, and graphite according to their respective composition and content. The dephosphorizer was based on Fe_tO–CaO–SiO_2–$CaCl_2$ slags and prepared with Fe_2O_3, CaO, $CaCl_2$, $Ca(OH)_2$, $CaCO_3$ powders (Note: SiO_2 was obtained by oxidizing silicon in the hot metal, $CaCl_2$ is better than CaF_2 in dephosphorization of medium-phosphorus hot metal [18]). All raw materials of the dephosphorizer were analytically pure, and the particle size of CaO, $Ca(OH)_2$, and $CaCO_3$ powders was 0.106 to 0.088 mm. The chemical compositions of the pig iron powder and the dephosphorizers are shown in Tables 1 and 2, respectively.

Table 1. Chemical composition of the pig iron powder (wt.%).

Composition	C	Si	Mn	P	S
Content	3.0	0.50	0.45	0.30	0.045

Table 2. Chemical composition of the dephosphorizer (wt.%).

No.	Composition				
	Fe_2O_3	CaO	$CaCl_2$	$Ca(OH)_2$	$CaCO_3$
A	31.3	49.1	19.6	—	—
B	27.1	—	17.0	56.0	—
C	22.6	—	14.1	—	63.3

2.2. Methods

In order to investigate the mass transfer of phosphorus when dephosphorizer only uses CaO, $Ca(OH)_2$, or $CaCO_3$ as its fixative, the numbers of dephosphorizers used in the experiment were A, B, and C, respectively, and dephosphorizer number was also used as experiment number.

The experiment process is as follows. At room temperature, an Al_2O_3 crucible (55 mm I.D. × 120 mm) was put into the T-1700VCB crucible furnace and kept warm when the furnace was heated to 1400 ± 20 °C, and then the paper-coated pig iron powder (600 g) was added to the crucible with an equal diameter glass tube. When the pig iron powder

was completely melted, the paper-wrapped dephosphorizer (A 62.0 g, B 71.8 g, or C 86.2 g) was added to the hot metal, and the hot-metal sample was collected by using a glass tub (6 mm I.D.) at different times. Finally, the surface of the cooled metal sample was polished, and a small amount of the metal filings was drilled, which was analyzed by the ICP-AES after acid leaching. Meanwhile, the slag sample was analyzed by the XRF after being ground into powder.

In the initial components, $n(Fe_2O_3) = 0.67n[Si] + 0.83n[P]$, $n_A(CaO) = n_B(Ca(OH)_2) = n_C(CaCO_3) = 2.68n[Si] + 12.68n[P]$, where n represents the molar amount of substance, ( ) and [] indicate that the substance is in the slag and hot metal, respectively. Subscripts A, B and C are dephosphorizer numbers.

3. Theoretical Analysis and Model Establishment

Generally, the dephosphorization process includes:

a. [P] diffuses from the hot-metal interior to the slag-metal interface;
b. [O] diffuses from the hot-metal or slag interior to the slag-metal interface;
c. (O^{2-}) diffuses from the slag interior to the slag-metal interface;
d. [P], [O], and (O^{2-}) react and form $(PO_4{}^{3-})$;
e. $(PO_4{}^{3-})$ diffuses from the slag-metal interface to the slag interior.

In the above process, the ion reaction of phosphorus transferred from hot metal to slag is as follows:

$$[P] + \frac{5}{2}[O] + \frac{3}{2}\left(O^{2-}\right) = \left(PO_4^{3-}\right) \quad (1)$$

Obviously, in this reaction, the mass transfer of phosphorus includes the transfer of [P] in the hot metal and $(PO_4{}^{3-})$ in the slag. Normally, in the two-film theory in liquid-liquid reaction, the slag-metal contact area A is mostly taken as a constant. However, in the actual reaction, the contact area between phosphorus and oxygen at the interface is not fixed.

As shown in Figure 1, with the oxidation and transfer (to the slag) of phosphorus at the slag-metal interface, the content of phosphorus in the hot metal continues to decrease, so the phosphorus diffused from the hot-metal interior to the slag-metal interface will be less and less, which will directly reduce the P–O contact area at the interface. In traditional dephosphorization models, the reaction area is directly replaced by the slag-metal contact area, which is difficult to reflect the effect of the decrease in hot-metal phosphorus content on P–O contact area. Therefore, according to the restrictive conditions of the reaction, it is more reasonable to use a "dynamic relative area" which is based on the slag-metal contact area and can reflect the change in P–O contact area relative to the initial value.

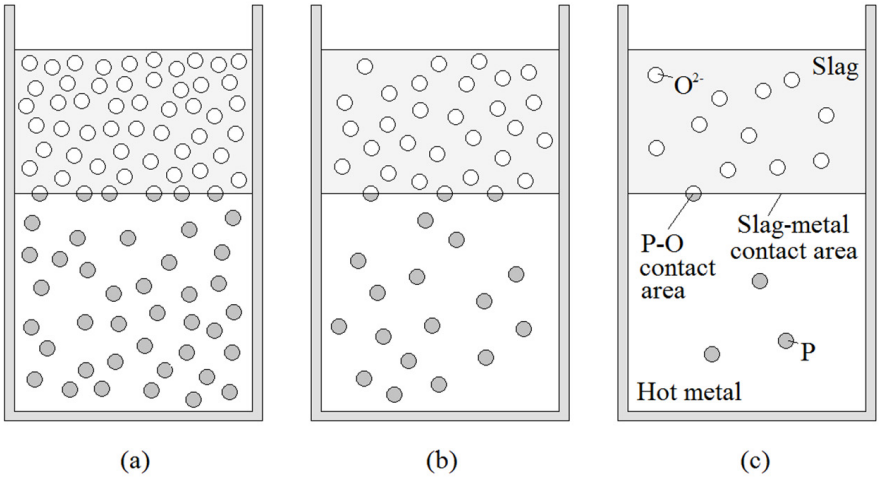

Figure 1. Relationship between P–O contact area and hot-metal phosphorus content with time. ((**a**) Initial stage, (**b**) middle stage, (**c**) final stage).

Since the content of oxygen (O^{2-}) in slag during dephosphorization is much higher than that of phosphorus in hot metal, the restrictive condition at this time is the phosphorus content in hot metal. Therefore, the use of "dynamic relative area" $\frac{[\%P]}{[\%P]^0}A$ ($[\%P]^0$ is the initial hot-metal phosphorus content during the selected dephosphorization period) can well reflect the relative decrease in P–O contact area in hot metal. At this time, the mass transfer flux equations of phosphorus in the hot metal and slag can be expressed as:

$$\frac{d[\%P]}{dt} = -\frac{[\%P]}{[\%P]^0}\frac{A}{W_m}\rho_m k_m\{[\%P] - [\%P]^*\} \quad (2)$$

$$\frac{d(\%P)}{dt} = -\frac{[\%P]}{[\%P]^0}\frac{A}{W_s}\rho_s k_s\{(\%P) - (\%P)^*\} \quad (3)$$

where [%P] and (%P) represent phosphorus content in the hot metal and slag, respectively, [%P]* and (%P)* represent phosphorus content in the hot metal and slag at the slag-metal interface. k_m and k_s are mass transfer coefficients in the hot metal and slag, respectively. ρ_m and ρ_s are the density of hot metal and slag, respectively. W_m and W_s are the mass of the hot metal and slag, respectively, and A is the slag-metal contact area.

Meanwhile, the mass balance equation of phosphorus in the dephosphorization process is as follows:

$$\frac{d(\%P)}{dt}W_s = -\frac{d[\%P]}{dt}W_m \quad (4)$$

Based on the above equations, the dephosphorization rate can be expressed as:

$$\frac{d[\%P]}{dt} = -\frac{A\rho_m}{[\%P]^0 W_m}\frac{1}{\frac{\rho_m}{\rho_s k_s L_P} + \frac{1}{k_m}}\{[\%P]^2 - [\%P]\frac{(\%P)}{L_P}\} \quad (5)$$

Among them, the phosphorus distribution ratio L_P is calculated by phosphorus content in the hot metal and slag when the reaction reaches equilibrium.

$$L_P = \frac{(\%P)^*}{[\%P]^*} \quad (6)$$

Because the mass transfer of phosphorus is affected by both the hot metal and slag, according to previous research, the overall mass transfer coefficient k_O is still defined as:

$$k_O = \frac{1}{\frac{\rho_m}{\rho_s k_s L_P} + \frac{1}{k_m}} \quad (7)$$

At any time during dephosphorization, the mass of phosphorus in the hot metal and slag should meet the following equation:

$$W_m[\%P] = W_m[\%P]^0 - W_s(\%P) \quad (8)$$

Finally, the dephosphorization kinetic model is as follows:

$$[\%P] = \frac{W_m[\%P]^0}{W_s L_P}\left(\frac{W_m}{W_s L_P} + 1 - e^{-\frac{A\rho_m k_O}{W_s L_P}t}\right)^{-1} \quad (9)$$

Moreover, referring to the definition of traditional mass transfer parameters ($A{\cdot}k_O$), a new expression of $A{\cdot}k_O$ can be obtained through deformation:

$$A \cdot k_O t = -\frac{W_s L_P}{\rho_m}\ln\left(-\frac{W_m}{W_s L_P}\frac{[\%P]^0}{[\%P]} + \frac{W_m}{W_s L_P} + 1\right) \quad (10)$$

For the follow-up analysis, referring to the definition of previous scholars, the expression on the right side of the equal sign of Formula (10) is still represented by "RHS".

4. Results and Discussion

4.1. Effect of "Dynamic Relative Area" on Fitting Deviation

In order to verify the rationality of the new dephosphorization model, the new and old models need to be compared and analyzed with the help of [%P]—time data in the literature. Since the dephosphorization model is based on the melting state of slag and hot metal, according to Mori's experiment method [10], his data will be more convincing. The fitting results of the two models to Mori's [%P]—time data are shown in Figures 2 and 3.

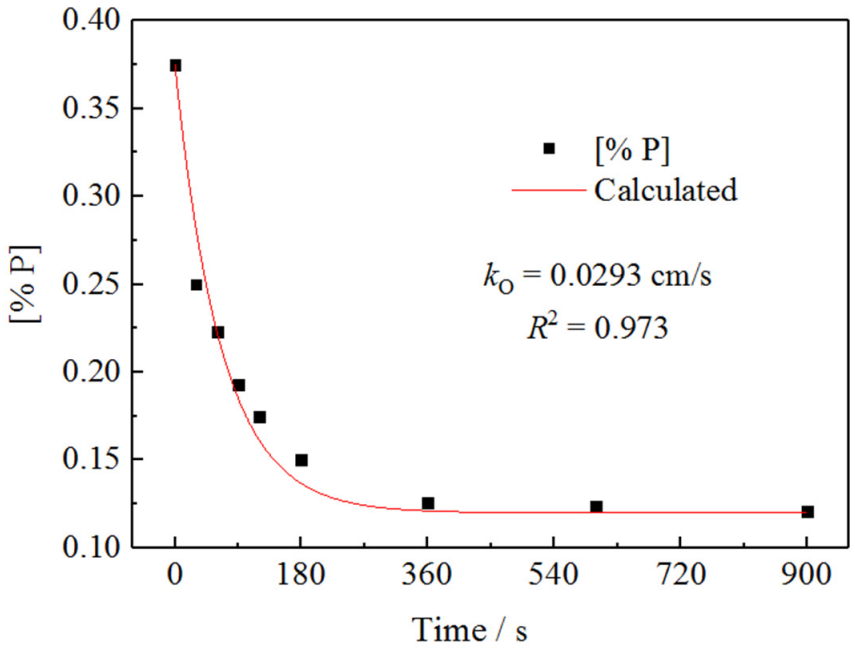

Figure 2. Fitting of Mori's dephosphorization data (old model reprinted from Ref. [12]).

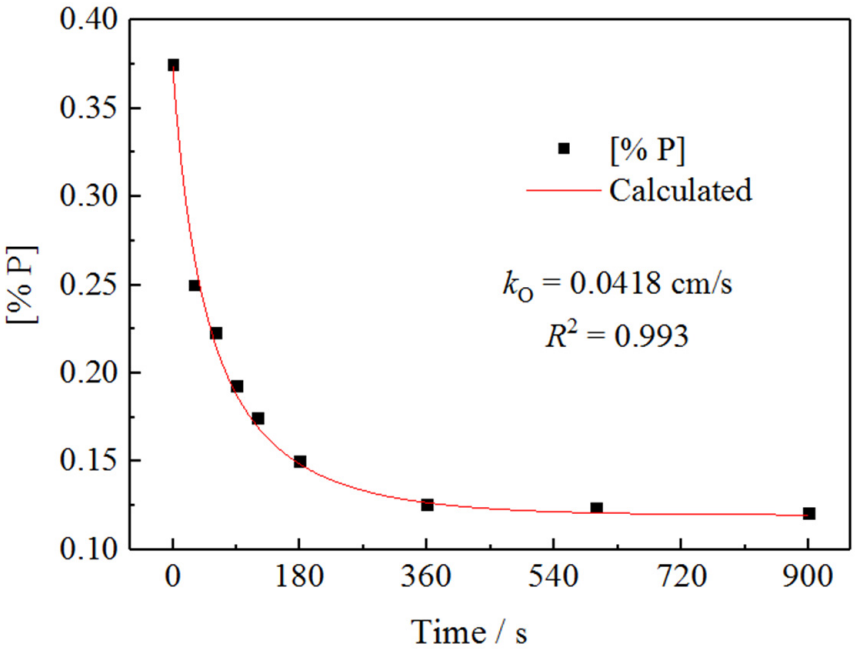

Figure 3. Fitting of Mori's dephosphorization data (new model).

Compared with Figures 2 and 3, the new dephosphorization model (the new model) shows a higher consistency with Mori's experimental data than the traditional dephosphorization model (the old model). After calculation, the determination coefficient R^2 (0.993) of the new model is also higher than that of the old model (0.973). Through further observation, it is found that the fitting curve of the old model presents a certain accuracy only after 360 s, while the fitting curve within 0 to 360 s deviates greatly from the experimental data. Comparatively speaking, the new model shows no obvious deviation during the whole dephosphorization period. Obviously, compared with the change in the phosphorus content in hot metal after 360 s, the phosphorus content within 0 to 360 s decreases faster, which means that the relative change value of P–O reaction area is larger, but the old model can not reflect this feature, so the k_O calculated by it has low credibility.

It should be noted that the k_O calculated by the new and old models are 0.0418 cm/s and 0.0293 cm/s, respectively. The k_O of the new model is significantly higher than that of the old model, indicating that the actual k_O should be higher after eliminating the interference of the P–O contact area change.

In short, compared with the traditional dephosphorization model, the rationality of the new dephosphorization model can be confirmed in relatively ideal experiments. Therefore, it is feasible to apply the new model to investigate the mass transfer of phosphorus.

4.2. Effect of "Dynamic Relative Area" on Mass Transfer Parameter

According to Manning's research [12], the mass transfer parameter ($A \cdot k_O$) should not change with time or composition. He believes that even if some dynamic interface phenomena may cause a distortion of the interface, the interface area will only increase temporarily without continuous and significant changes. However, the $A \cdot k_O$ calculated by traditional dephosphorization models usually shows an obvious downward trend, which has been confirmed by the research results of Manning, Diao, and Ji. Therefore, the rationality of the new model can be judged indirectly by investigating the effect of "dynamic relative area" on $A \cdot k_O$.

First, it is based on Mori's RHS-time data, two models are used to calculate and fit them respectively, and Figures 4 and 5 were obtained. In the figures, the RHS-time fitting curves are divided into three stages (0 to 120 s, 120 to 360 s, 360 to 900 s), and the average values of $A \cdot k_O$ in each stage are marked.

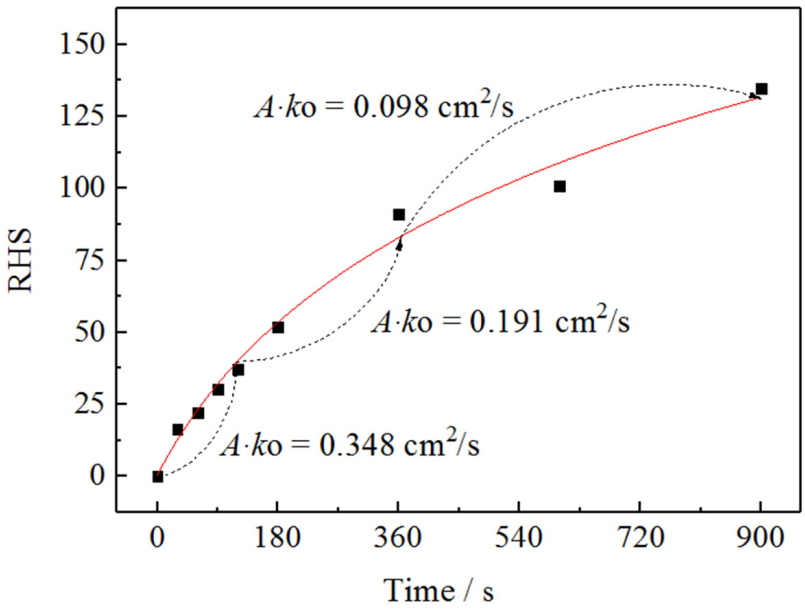

Figure 4. Relationship between RHS and time in Mori's experiment (old model).

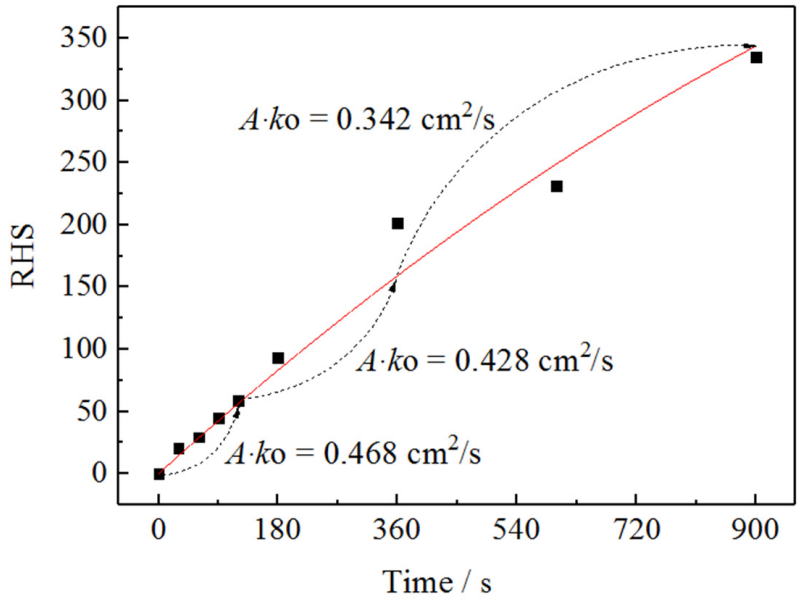

Figure 5. Relationship between RHS and time in Mori's experiment (new model).

Figures 4 and 5 show the relationship between RHS and time fitted by two models, respectively. The fitting curves obtained by two models are obviously different. There is a more obvious "bulge" in Figure 4, while the curve in Figure 5 is relatively straight, that is, its slope ($A{\cdot}k_O$) fluctuates less, indicating that as the dephosphorization reaction proceeds, the decrease in P–O contact area caused by the hot-metal phosphorus content decrease indeed affects $A{\cdot}k_O$, and mainly in two aspects of numerical value and stability.

In terms of numerical value, the $A{\cdot}k_O$ of the new and old models in three stages are 0.486, 0.428, 0.342 cm^2/s and 0.348, 0.191, 0.098 cm^2/s, respectively. The $A{\cdot}k_O$ of the new model are higher than those of the old model, indicating that after considering the effect of "dynamic relative area", real $A{\cdot}k_O$ tends to be higher, and the decrease is not obvious with the reaction going on.

In terms of stability, K is temporarily used to represent the change rate of the $A{\cdot}k_O$ between the initial and final points of the RHS-time curve, which is defined as:

$$K = \frac{(A \cdot k_O)_{final} - (A \cdot k_O)_{iniial}}{(A \cdot k_O)_{iniial}} \tag{11}$$

The smaller the K, the more stable the curve. Through the calculation, the K of the new and old models are 0.415 and 0.856, respectively, and the K of the new model curve is obviously smaller, that is, its stability is higher. It is obvious that this result, to some extent, explains the phenomenon that has perplexed some scholars about the abnormal decline of $A{\cdot}k_O$ for a long time.

However, considering that the K of the new model curve is not zero, the viewpoint of "dynamic relative area" is still not enough to explain all the phenomena.

4.3. Effects of CaO and Its Derivatives on Mass Transfer of Phosphorus

The previous discussion has proved the rationality of the new dephosphorization model from two aspects, including the effect of "dynamic relative area" on fitting deviation and mass transfer parameter. Therefore, it is feasible to investigate the mass transfer of phosphorus in CaO and its derivatives using the new model. Based on the data of experiments A, B, and C, the new model is used to draw Figure 6.

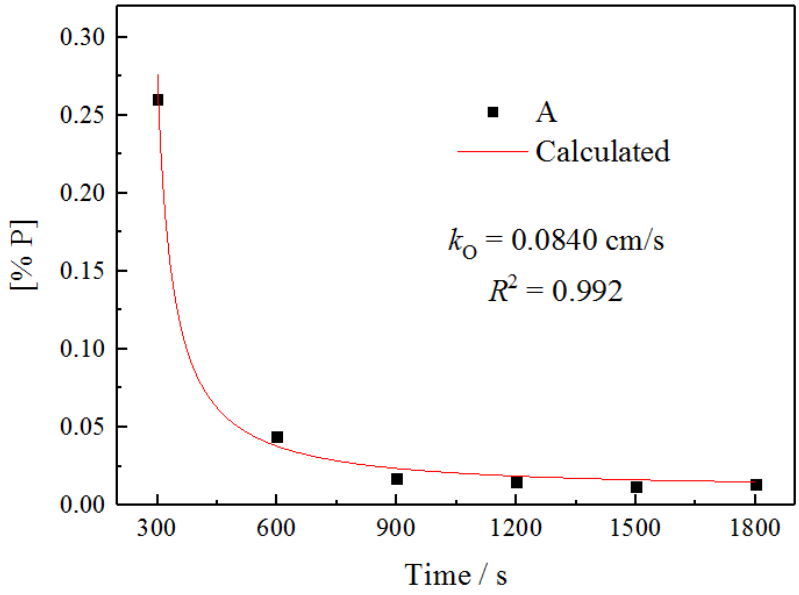

Figure 6. Fitting results of experiment A data.

Figures 6–8 demonstrate the fitting results of the new dephosphorization model to the [%P]—time data in experiments A, B, and C. Considering the interference of the dephosphorizer melting process, the new model only fits the experimental data after 300 s. As can be seen, the hot-metal phosphorus content in three experiments decreases rapidly in the first 300 s and tends to be a constant with the reaction progress, but the k_O in each experiment is significantly different. According to Figures 6–8, the k_O of three experiments are 0.0840 cm/s, 0.0216 cm/s, and 0.0363 cm/s, respectively. The k_O of A is much higher than that of B and C, indicating that the existence of $Ca(OH)_2$ and $CaCO_3$ is not conducive to mass transfer of phosphorus.

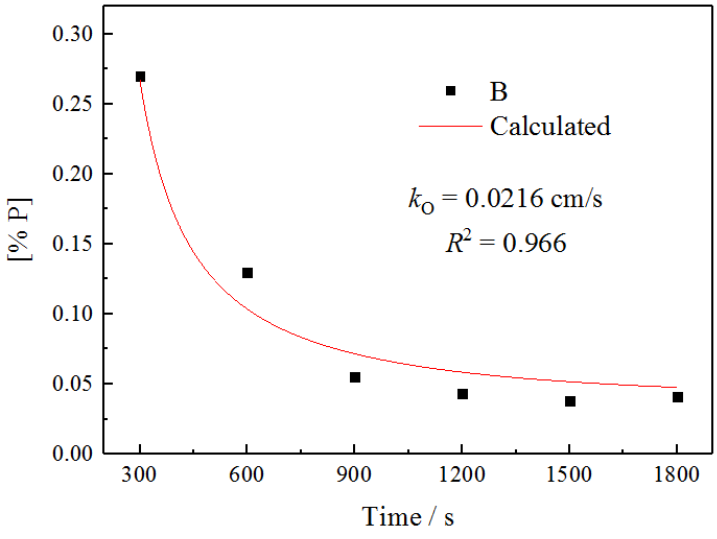

Figure 7. Fitting results of experiment B data.

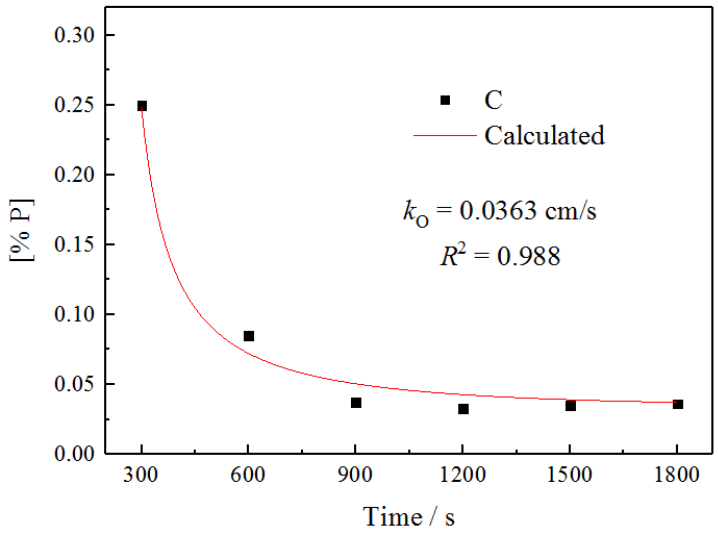

Figure 8. Fitting results of experiment C data.

From the perspective of the dephosphorization thermodynamics, both $CaCO_3$ and $Ca(OH)_2$ will absorb heat and decompose under high-temperature conditions, thereby reducing the temperature of the hot metal and slag, which is very beneficial to dephosphorization [2,3]. Meanwhile, the decomposition heat of $CaCO_3$ ($\triangle_r H^\theta_m$ (1673 K) = 146.12 kJ/mol) is obviously higher than that of $Ca(OH)_2$ ($\triangle_r H^\theta_m$ (1673 K) = 21.51 kJ/mol). Therefore, the thermodynamic advantages of CaO, $Ca(OH)_2$, and $CaCO_3$ increase in turn.

However, in order to realize the oxidation of phosphorus, the movement of oxidants in slag is also very important, which is directly related to the fluidity of slag. First of all, the melting points of $Ca(OH)_2$, $CaCO_3$ and CaO increase in turn, which causes their fluidity to decrease in turn at the same temperature. Secondly, when $CaCO_3$ and $Ca(OH)_2$ are decomposed at high temperatures, the greater the decomposition heat is, the more obvious the hindrance to the heating and melting of slag is.

Specifically, the P–O reaction in experiment B had a moderate thermodynamic condition, and the slag fluidity was the highest in the three experiments. However, $Ca(OH)_2$ would inevitably produce excessive bubbles in the decomposition process, which caused continuous and serious foaming of the slag. Meanwhile, because the slag and hot metal were not stirred in the experiment, even if $Ca(OH)_2$ was completely decomposed, most of the foamed slag would be suspended above the hot metal because of its adsorption on the inner wall of the crucible, so it was difficult to contact the hot metal (this has been confirmed in the experiment, and resulted in a relatively higher final phosphorus content). As a result, the foam formed by $Ca(OH)_2$ expanded the mass transfer distance of O^{2-}, and even hindered the reaction of some slag and hot metal, eventually resulting in a very low k_O.

Comparatively speaking, experiment C had an obvious thermodynamic advantage in reducing the P–O reaction temperature, but due to the excessive heat absorption of $CaCO_3$ in the decomposition process, the heat required for slag melting had to be restricted, which directly reduced the fluidity of the slag. In addition, according to Zhong et al. [5], when the temperature exceeds 850 °C, there will be an obvious sintering phenomenon in the decomposition process of $CaCO_3$, which is consistent with the surface hardening and cracking of slag until the end of the experiment. At this time, the conversion rate of CaO decreased, and the fluidity of slag became worse. Both cases seriously hindered the diffusion of O^{2-} and PO_4^{3-} in the slag. As a result, the k_O was only slightly higher than that in experiment B.

Finally, as a reference, experiment A had no thermodynamic advantage, and the fluidity of the slag was the lowest among the three because of the high melting point of CaO. Fortunately, compared with $Ca(OH)_2$ and $CaCO_3$, CaO did not absorb excessive heat or cause foaming slag formation during heating. Therefore, it was obvious that the

diffusion resistance of O^{2-} and PO_4^{3-} in the slag was relatively small, and a high k_O was easy to obtain.

4.4. Effect of Slag Viscosity on Transfer of Phosphorus Mass

To further evaluate the reliability of the results obtained, it is necessary to understand the change in slag viscosity during dephosphorization. The chemical compositions of the final hot metal and slags are shown in Tables 3 and 4, respectively.

Table 3. Chemical composition of the final hot metal (wt.%).

No.	Composition				
	C	Si	Mn	P	S
A	2.03	0.003	0.13	0.013	0.013
B	2.18	0.007	0.20	0.041	0.009
C	2.16	0.008	0.21	0.036	0.010

Table 4. Chemical composition of the final slag (wt.%).

No.	Composition							
	CaO	SiO_2	FeO	MnO	MgO	Al_2O_3	P_2O_5	$CaCl_2$
A	35.32	17.21	3.03	3.97	1.65	11.88	6.74	16.23
B	39.07	11.54	5.11	3.14	0.704	13.87	6.07	15.07
C	39.97	9.55	5.12	3.04	0.586	13.52	6.02	15.82

It can be seen from Tables 3 and 4 that other elements besides P in hot metal were also partially oxidized and entered the slag. Among them, Si and Mn have a relatively greater effect on the mass transfer of phosphorus. Generally, the viscosity of slag is two orders of magnitude higher than that of hot metal, so its effect on mass transfer of phosphorus is much greater than that of hot metal. In view of this, the following mainly investigates the effect of Si and Mn on slag viscosity.

As we all know, the viscosity of basic steelmaking slag is relatively small in homogeneous state and decreases with increasing FeO content. Because both the basicity of slag (>2) and FeO content (>10 wt.%) are high, the Si–O complexions in it mostly exist in the smallest structural unit SiO_4^{4-}, and the melting point of this slag is also relatively low [19].

However, with the progress of dephosphorization reaction, the FeO content will decrease, while the contents of SiO_2 and MnO will increase in the slag. Among them, the slag viscosity can increase with the increase in SiO_2 content and decrease with the increase in MnO content. Considering the reduction in FeO content and the changes in other components in the slag, their final effect is often difficult to determine.

Nevertheless, it is feasible to use empirical Formula (12) [19] to roughly judge the viscosity of the initial and final slag.

$$\ln \eta = \frac{1}{0.15 - 0.44\Lambda} - \frac{1.77 + 2.88\Lambda}{T} \tag{12}$$

where, η represents the viscosity of the slag, Λ represents the optical basicity of the slag, and T represents the temperature.

For the convenience of analysis, the effect of flux in the experiment is not considered temporarily, and it is assumed that all slag components were completely dissolved at 1400 °C and the temperature remained constant. Through calculation, the viscosity of the initial slag is 0.0073 Pa·s, and viscosities of final slag A, B, and C are 0.0011, 0.0019 and 0.0023 Pa·s, respectively. It is not difficult to find that the dephosphorization process reduced the slag viscosity, and the final slag viscosity in experiment A was significantly lower than that in experiments B and C, which explains the reason for the larger k_O obtained in experiment A to a certain extent.

In addition, the basicity of the final slags ($R = w(CaO)/(w(SiO_2) + w(P_2O_5))$ is 1.47, 2.22, and 2.57, respectively. They all have a certain deviation from the set ideal value, but considering the heterogeneous slag composition and sampling error, this is still acceptable. Obviously, the lower basicity in experiment A is due to its higher dephosphorization efficiency than experiments B and C.

5. Conclusions

The main results are as follows:

(1) According to the change in hot-metal phosphorus content during dephosphorization, a new dephosphorization kinetic model has been established by introducing a new concept "dynamic relative area". The test of [%P]—time data in the related literature shows that the consistency of the new model is higher than that of the traditional model.

(2) The research on the mass transfer parameter shows that neglecting the decrease in P–O contact area at the slag-metal interface during the reaction is an important reason for the fluctuation in the $A \cdot k_O$ calculated by traditional dephosphorization models.

(3) In the research on CaO and its derivatives, the k_O values affected by CaO, $Ca(OH)_2$, and $CaCO_3$ are 0.0840, 0.0216, and 0.0363 cm/s, respectively.

(4) The dephosphorization reaction can reduce the viscosity of the slags and has a greater effect on the viscosity of CaO-based slag, which explains the reason for its larger k_O to a certain extent.

(5) The establishment of the new dephosphorization kinetic model can provide feasibility for the research on the mass transfer mechanism of phosphorus under the action of CaO and its derivatives. The results have shown that the existence of $Ca(OH)_2$ and $CaCO_3$ is extremely disadvantageous to mass transfer of phosphorus in slag, which needs to be avoided as much as possible.

Author Contributions: Conceptualization, G.S.; methodology, G.S.; validation, G.S.; formal analysis, G.S.; investigation, G.S.; data curation, G.S.; writing—original draft preparation, G.S.; writing—review and editing, X.X.; visualization, G.S.; supervision, X.X.; project administration, X.X.; funding acquisition, X.X. All authors have read and agreed to the published version of the manuscript.

Funding: This research was funded by [Wuhan Science and Technology Bureau] grant number [2016060101010071] And The APC was funded by [Wuhan University of science and technology].

Data Availability Statement: Not applicable.

Acknowledgments: We would like to acknowledge Wuhan Science and Technology Plan Project (2016060101010071) for financial support.

Conflicts of Interest: The authors declare no conflict of interest.

References

1. Yang, R.G. Test and Analysis of Calcium Oxide Content and Reactivity Changes of Active Lime during Its Storage and Transport. *Foreign Refract.* **2013**, *38*, 18–19.
2. Lu, S.Q.; Wu, S.F. Advances in Calcium Carbonate Thermal Decomposition. *J. Chem. Ind. Eng.* **2015**, *66*, 2895–2902.
3. Long, X.F.; Wu, J. Thermal Decomposition Kinetics of Thermochemical Energy Storage System $Ca(OH)_2/CaO$. *J. South China Univ. Technol. Nat. Sci. Ed.* **2014**, *42*, 75–81.
4. Cao, K. Determination of Calcium Hydroxide and Calcium Carbonate. *Synth. Lubr.* **2006**, *33*, 16–18.
5. Zhong, Z.P.; Marnie, T.; Zhang, M.Y.; Li, D.J.; Xu, Y.N.; Jin, B.S.; Lan, J.X.; Zhang, D.K. Experimental Study on Pyrolysis of Caroline Limestone. *J. Combust. Sci. Technol.* **2001**, *7*, 110–114.
6. Kitamura, S. Importance of Kinetic Models in the Analysis of Steelmaking Reactions. *Steel Res. Int.* **2010**, *81*, 766–771. [CrossRef]
7. Kitamura, S.Y.; Shibata, H.; Maruoka, N. Kinetic Model of Hot Metal Dephosphorization by Liquid and Solid Coexisting Slags. *Steel Res. Int.* **2008**, *79*, 586–590. [CrossRef]
8. Zhang, X.; Xie, B.; Li, H.Y.; Diao, J.; Ji, C.Q. Coupled Reaction Kinetics of Duplex Steelmaking Process for High Phosphorus Hot Metal. *Ironmak. Steelmak.* **2013**, *40*, 282–289. [CrossRef]
9. Tian, Z.H. Technology and Theory of Molten Steel Deep Dephosphorization out of Converter for Production of Ultra–low Phosphorus Steel. Ph.D. Thesis, University of Science and Technology Beijing, Beijing, China, 2005; p. 141.
10. Mori, K.; Doi, S.; Kaneko, T.; Kawai, Y. Rate of Transfer of Phosphorus between Metal and Slag. *Trans. Iron Steel Inst. Jpn.* **1978**, *18*, 261–268. [CrossRef]

11. Manning, C.P. Behavior of Phosphorus in DRI/HBI during Electric Furnace Steelmaking. Ph.D. Thesis, Carnegie Mellon University, Pittsburgh, PA, USA, 2000; p. 175.
12. Manning, C.P.; Fruehan, R.J. The Rate of the Phosphorous Reaction Between Liquid Iron and Slag. *Metall. Mater. Trans. B* **2013**, *44*, 37–44. [CrossRef]
13. Diao, J.; Liu, X.; Zhang, T.; Xie, B. Mass transfer of phosphorus in high-phosphorus hot-metal refining. *Int. J. Miner. Met. Mater.* **2015**, *3*, 249–253. [CrossRef]
14. Diao, J. Applied Fundamental Research on Medium and High Phosphorus Hot Metal Refining by Duplex Process in Converter. Ph.D. Thesis, Chongqing University, Chongqing, China, 2010; p. 62.
15. Ji, C.Q. Study on Dephosphorization Kinetics of High-phosphorus Hot-metal by CaO–SiO_2–FetO–Na_2O(Al_2O_3) Slag. Master's Thesis, Chongqing University, Chongqing, China, 2010; p. 41.
16. Wang, Z.J.; Shu, Q.F.; Sridhar, S.; Zhang, M.; Guo, M.; Zhang, Z.T. Effect of P_2O_5 and FetO on the Viscosity and Slag Structure in Steelmaking Slags. *Metall. Mater. Trans. B* **2015**, *46*, 758–765. [CrossRef]
17. Gu, K.; Dogan, N.; Coley, K.S. Dephosphorization Kinetics between Bloated Metal Droplets and Slag Containing FeO: The Influence of CO Bubbles on the Mass Transfer of Phosphorus in the Metal. *Metall. Mater. Trans. B* **2017**, *48*, 2984–3001. [CrossRef]
18. Wen, Z.J.; Wu, J.; Ceng, M.J. Study on Dephosphorization Pretreatment of Hot Metal. *China New Technol. Prod.* **2012**, *22*, 88–89.
19. Huang, X.H. *Principles of Iron and Steel Metallurgy*, 4th ed.; Metallurgical Industry Press: Beijing, China, 2013; p. 317.